NMR Spectroscopy

International Edition: DOI: 10.1002/anie.201608559
German Edition: DOI: 10.1002/ange.201608559

Uncovering Key Structural Features of an Enantioselective Peptide-Catalyzed Acylation Utilizing Advanced NMR Techniques

Eliška Procházková, Andreas Kolmer, Julian Ilgen, Mira Schwab, Lukas Kaltschnee, Maic Fredersdorf, Volker Schmidts, Raffael C. Wende, Peter R. Schreiner, and Christina M. Thiele**

Abstract: *We report on a detailed NMR spectroscopic study of the catalyst-substrate interaction of a highly enantioselective oligopeptide catalyst that is used for the kinetic resolution of trans-cycloalkane-1,2-diols via monoacylation. The extraordinary selectivity has been rationalized by molecular dynamics as well as density functional theory (DFT) computations. Herein we describe the conformational analysis of the organocatalyst studied by a combination of nuclear Overhauser effect (NOE) and residual dipolar coupling (RDC)-based methods that resulted in an ensemble of four final conformers. To corroborate the proposed mechanism, we also investigated the catalyst in mixtures with both trans-cyclohexane-1,2-diol enantiomers separately, using advanced NMR methods such as T_1 relaxation time and diffusion-ordered spectroscopy (DOSY) measurements to probe molecular aggregation. We determined intramolecular distance changes within the catalyst after diol addition from quantitative NOE data. Finally, we developed a pure shift EASY ROESY experiment using PSYCHE homodecoupling to directly observe intermolecular NOE contacts between the trans-1,2-diol and the cyclohexyl moiety of the catalyst hidden by spectral overlap in conventional spectra. All experimental NMR data support the results proposed by earlier computations including the proposed key role of dispersion interaction.*

Acyl transfer belongs to one of the most significant chemical reactions occurring in biological systems as well as in organic synthesis, where it is widely used in enantioselective catalysis.[1] Kinetic resolution of chiral secondary alcohols through acylation is a powerful tool for preparing optically pure compounds for chemical syntheses.[2] For a long time, enzymes played a key role in organic synthesis, for example, lipases or acylases have been employed for acylation of structurally different classes of secondary alcohols.[3] Within the last two decades peptide-based catalysts have been discovered and established as versatile low-molecular-weight alternatives to enzymes.[4] They can form enzyme-like active sites and can interact specifically with substrates.[4b,5] Such catalysts are considered very efficient owing to their high structural diversity and their ability to form multiple non-covalent interactions simultaneously, for example, hydrogen bonds, van der Waals as well as electrostatic interactions. Although this biomimetic approach works well for a variety of racemic alcohols, the effectivity of the kinetic resolution of *trans*-cycloalkane-1,2-diols had been astonishingly low.

This situation changed with the introduction of the novel lipophilic peptide-based catalyst Boc-L-(π-Me)-His-^{A}Gly-L-Cha-L-Phe-OMe[6] (**1**), where ^{A}Gly represents γ-aminoadamantane carboxylic acid (Scheme 1). The designed oligopeptide contains a non-natural adamantyl amino acid to increase rigidity and solubility in organic solvents. The nucleophilic *N*-π-methylhistidine moiety is deemed catalytically active during the enantioselective acetyl transfer.[4a] Finally, the unnatural amino acid (*S*)-cyclohexylalanine is proposed to enable dispersion interactions with the substrate that build the basis for high selectivities.[7] To rationalize the origin of the extraordinary high stereoselectivity of peptide catalyst **1**, molecular mechanics (MMFF) was employed and a dynamic binding-pocket within the acylated tetrapeptide intermediate was proposed.[7] In subsequent work,[7,8] the transition structures of the tetrapeptide–diol complex were optimized by DFT [M06-2X/6-31 + G(d,p)] computations taking into account medium-range correlation effects.[9] However, there was no experimental evidence confirming the proposed mechanism and explaining the extraordinary enantiodiscrimination up to now.

Herein, we investigate the conformational ensemble of peptide catalyst **1** by a combination of NOE[10] and RDC[11] data to extract NMR parameters directly connected to molecular structure (distances, angles). Furthermore, the differential interactions of **1** with the two enantiomers of *trans*-cyclohexane-1,2-diol (**2**) are explored to gain insights into the enantioselective recognition process.

To investigate **1** under conditions as close to the reaction conditions as possible, as little as 2 mg of **1** were dissolved in deuterated toluene (3.2 mmol L^{-1}). As the signals were severely broadened (see Supporting Information) at the

[*] Dr. E. Procházková, Dr. A. Kolmer, J. Ilgen, M. Schwab, Dr. L. Kaltschnee, Dr. M. Fredersdorf, Dr. V. Schmidts, Prof. Dr. C. M. Thiele
Clemens-Schöpf-Institut für Organische Chemie und Biochemie
Technische Universität Darmstadt
Alarich-Weiss-Strasse 16, 64287 Darmstadt (Germany)
E-mail: cthiele@thielelab.de
Dr. R. C. Wende, Prof. Dr. P. R. Schreiner
Institut für Organische Chemie
Justus-Liebig-Universität
Heinrich-Buff-Ring 17, 35392 Giessen (Germany)
E-mail: prs@uni-giessen.de
Dr. E. Procházková
On leave from Institute of Organic Chemistry and Biochemistry, Academy of Sciences of the Czech Republic
Flemingovo nám. 2, 166 10, Prague (Czech Republic)
Supporting information and the ORCID identification number(s) for the author(s) of this article can be found under http://dx.doi.org/10.1002/anie.201608559.

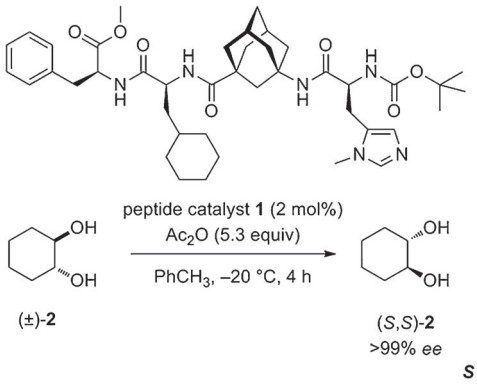

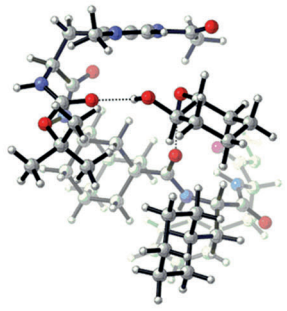

Scheme 1. Kinetic resolution using the tetrapeptide catalyst **1**, (*R,R*)-*trans*-cyclohexane-1,2-diol is acetylated preferentially (left). The dynamic binding pocket in the acylium ion/catalyst adduct with (*R,R*)-**2** proposed by computation (right);[7] dotted lines denote proposed H-bonds. Note the close proximity of the cyclohexyl moiety of **1** to **2** (dispersion interactions).

temperature associated with the highest selectivity ($S > 50$ at −20 °C), we conducted the experiment at 27 °C, the temperature at which lines are sharp and selectivity is still high ($S = 23$ at room temperature). Quantitative distance information was obtained from 1D selective NOE experiments[12] as well as 2D EASY ROESYs (efficient adiabatic symmetrized rotating frame Overhauser effect spectroscopy)[13] recorded as a series of measurements differing in mixing-time values. These served for the construction of PANIC[14] (peak amplitude normalization for improved cross-relaxation) plots, which permit the use of data points acquired with much longer mixing times and improves the accuracy of distances obtained. RDC data involve the coupling measurements of isotropic as well as anisotropic samples. To obtain the anisotropic samples the compound in question needs to be oriented with respect to the magnetic field by using so called alignment media. Few alignment media are compatible with both toluene and **1**. We succeeded in using an anisotropically swollen gel of thermally cross-linked (via divinylbenzene) polystyrene[15] (27.4 mmol L^{-1} of **1**). One-bond C–H coupling data ($^1J_{C\text{-}H}/^1D_{C\text{-}H}$) obtained from clean in-phase HSQC (CLIP-HSQC)[16] spectra, as well as long-range coupling C–H data ($^nJ_{C\text{-}H}/^nD_{C\text{-}H}$) obtained from HETLOC (determination of heteronuclear long range couplings)[17] were used in the structure elucidation process (see Supporting Information for representative PANIC plots, ROE derived distances, and RDCs). Having obtained these complementary structural parameters, the next step in the structure elucidation process was to find conformers or conformer ensembles that are in agreement with the experimental data. For RDCs in flexible organic compounds this is usually achieved by fitting the experimental data via singular value decomposition (SVD)[18] to ensembles of computed structures (e.g., DFT).[19] The ensemble with the best fit is considered to be the most probable (minimal) ensemble.

When considering the constitution of **1** as well as the number of low-energy structures in the computations, appreciable flexibility is expected. Therefore, we searched for an ensemble of conformers that was in accordance with ROE and RDC data simultaneously. All our attempts failed as the ensemble with the best agreement between experimental and calculated distances/structures was different for ROEs and RDCs. Further attempts to solve this problem by optimizing the MMFF structures at the B3LYP/6-31 + G(d,p) level or generating additional structures using the OPLS2.1[20] force field (as implemented in MacroModel)[21] led to the same results. In total we examined 660 structures, only 184 of which were redundant (present in different sets of structures obtained by different methods). Thus, a change in strategy was necessary.

The structures were analyzed in terms of dihedral angle ranges present and clustered accordingly (see Supporting Information). The fact that all six possible dihedral angle ranges are populated in the computed structures for most of the dihedral angles points toward a full coverage of the conformational space by the computations. We decided to employ a stepwise construction procedure and divided **1** into two parts with rigid ^{A}Gly as the obvious incision. For the "left hand" side (Phe-Cha part) nine and for the "right hand" side (His part) five dihedral angles were identified as relevant parts of the "backbone", respectively. Out of each dihedral-angle range for any relevant dihedral angle, one structure was chosen and the resulting ensemble was successively probed using the ROE data for these junctions (for details see Supporting Information). This led to four populated conformers for the Phe-Cha part and three populated conformers for the His part. The ROE-derived ensemble of the Phe-Cha part was then subjected to a multi-conformer single tensor (MCST) evaluation using the RDC data of the respective side.[19a] Although it is necessary to adjust the population of the conformers to obtain a good fit of the RDC data, it is nevertheless very reassuring that the conformers describing the RDC data sufficiently well are among those obtained from ROE data. The same cross check is impossible for the His part, owing to a too small number of RDCs available. In the next step, we joined the two parts: for which the global information content of RDCs is most helpful. Additionally, a number of inter-domain ROEs were also obtained, albeit with larger errors (see Supporting Information). The four conformers of the Phe-Cha part and the three conformers of the His part were then probed with all RDC data in a MCST analysis as well as with ROE data. According to the RDC analysis, four conformers are populated (Figure 1); among those, three are also populated in the ROE analysis (although populations differ). Thus, we concluded that we have obtained an ensemble of conformers that is in accordance with ROE and RDC data. This ensemble confirms the pocket-like structure of **1** proposed computationally (for comparison see Supporting Information).

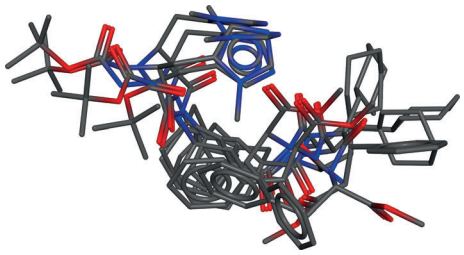

Figure 1. Four final conformers of peptide **1** obtained by a combination of ROE and RDC data.

After having verified the pocket-like shape of **1**, we attempted to acquire structural evidence for the enantioselective recognition of diol **2** by **1**. Mixtures of **1** with **2** in [D_8]toluene (both enantiomers separately) were prepared at two different concentrations of **1** (19.3 and 38.6 mmol L^{-1}): A significant dependence of the chemical shifts on concentration was observed (see Supporting Information), thus, it is essential to compare the samples at the same concentration. To study the degree of aggregation between **1** and the enantiomers of diol **2**, we measured the T_1 relaxation times and conducted DOSY experiments.

In general, bigger molecules or molecular complexes tend to display higher values of correlation time τ_C and this quantity is directly connected to relaxation time constants. Therefore, significant differences in T_1 could be helpful in deciding whether there is dynamic catalyst–substrate complex formation. For this purpose, we selected the well-separated NMR signal H-1 of **2** (CH proton neighboring the OH group; chemical shift ca 3.3 ppm, see Supporting Information). The T_1 of **2** in a mixture with **1** is significantly lower (ca 2.5 s) than for **2** alone (10.5 s). No significant difference in T_1 between the samples containing (*R*,*R*)-**2** and (*S*,*S*)-**2** was found though (2.5 and 2.6 s, respectively). On the other hand, the T_1 of **1** without and with **2** did not change significantly (1.58 and 1.60 s, respectively, see Supporting Information). T_1 relaxation time data suggest that there is an interaction between **1** and **2**, but no evidence was found for preferential binding of one of the enantiomers.

To support this interaction hypothesis, we measured DOSY spectra, where the chemical shift is correlated with the diffusion coefficient. We hoped to see different behavior of the enantiomeric diols **2** in mixtures with **1** in terms of different complex formation. At room temperature, we observed the same trend in both diol enantiomer mixtures. The diffusion coefficient of **2** is approximately three times higher than that of **1** ($D_{diol} = X D_{cat}$, with $X \approx 3$). We also measured D at the same temperature at which the catalytic reaction works best (−20 °C) and observed (Table 1) that ΔX ($X_{300K} - X_{253K}$) for (*S*,*S*)-**2** is significantly higher (0.70) than that for (*R*,*R*)-**2** (0.35). These results indicate that after a temperature change, the complex of **1** with *R*,*R*-(**2**) still behaves similarly, on the other hand, the complex with (*S*,*S*)-**2** displays larger changes. This could point towards a tighter complex in the case of (*R*,*R*)-**2**.

Table 1: The diffusivity ratios ($X = D_{diol}/D_{cat.}$) of the catalyst **1** and diols **2** at two different temperatures (room temperature and the reaction temperature).

Enantiomer	X_{300K}	X_{253K}	ΔX
(*R*,*R*)-**2**	2.96	2.61	0.35
(*S*,*S*)-**2**	3.09	2.39	0.70

To investigate whether structural changes occur in **1** after diol addition, we measured quantitative selective 1D NOE spectra (analyzed by PANIC plots). We extracted intramolecular distances and found significant changes between **1** alone and after the addition of **2**. Again, as in the case for the chemical shifts, we observed a dependence of intramolecular distances on concentration (see Supporting Information), thus, it is indispensable to compare samples with the same concentration only. The most significant changes are observed in the case of (*R*,*R*)-**2** at the His part of **1** (H-26, H-27, and H-28, see Supporting Information for corresponding PANIC plots). Interestingly, this is also the moiety that is responsible for the acetyl transfer. In Figure 2, these data are displayed as

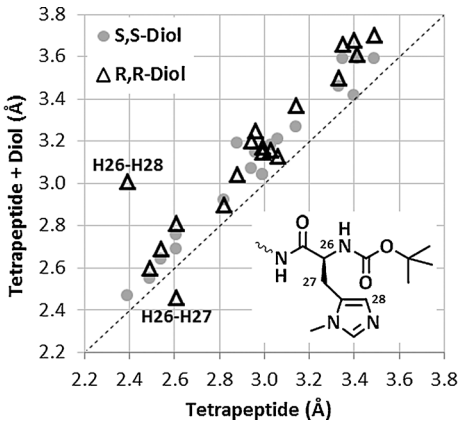

Figure 2. Intramolecular distances of **1** without and with addition of **2** as extracted from quantitative 1D NOE measurements. (*R*,*R*)-**2** addition (triangles) causes significantly larger changes in the structure of **1** than the addition of (*S*,*S*)-**2** (circles). The error of measurement was estimated to be not higher than 0.2 Å.

a correlation between intramolecular distances of **1** alone and in mixtures with **2**. After (*R*,*R*)-**2** addition (Figure 2, triangles), the H26–H28 distance is up to 0.6 Å larger, on the other hand, the H26–H27 distance is smaller. This means that an addition of (*R*,*R*)-**2** causes more significant structural changes of **1** than (*S*,*S*)-**2** (Figure 2, circles), in accordance with the preferential acetylation of (*R*,*R*)-**2**.[6,7]

In 1D NOE spectra, it was also possible to identify intermolecular contacts between **2** and the catalytically active His part of **1** (see Supporting Information). This observation led us to the idea to examine whether the observed intermolecular interactions are in accordance with the dispersion interactions[22] proposed by M06-2X/6-31 + G(d,p) computations.[7] However, this necessitated the development of a novel NMR spectroscopic method.

As the aliphatic region in which we expected intermolecular interactions (0.9–2.1 ppm) is overcrowded, we simplified the spectra using homonuclear decoupling (pure shift

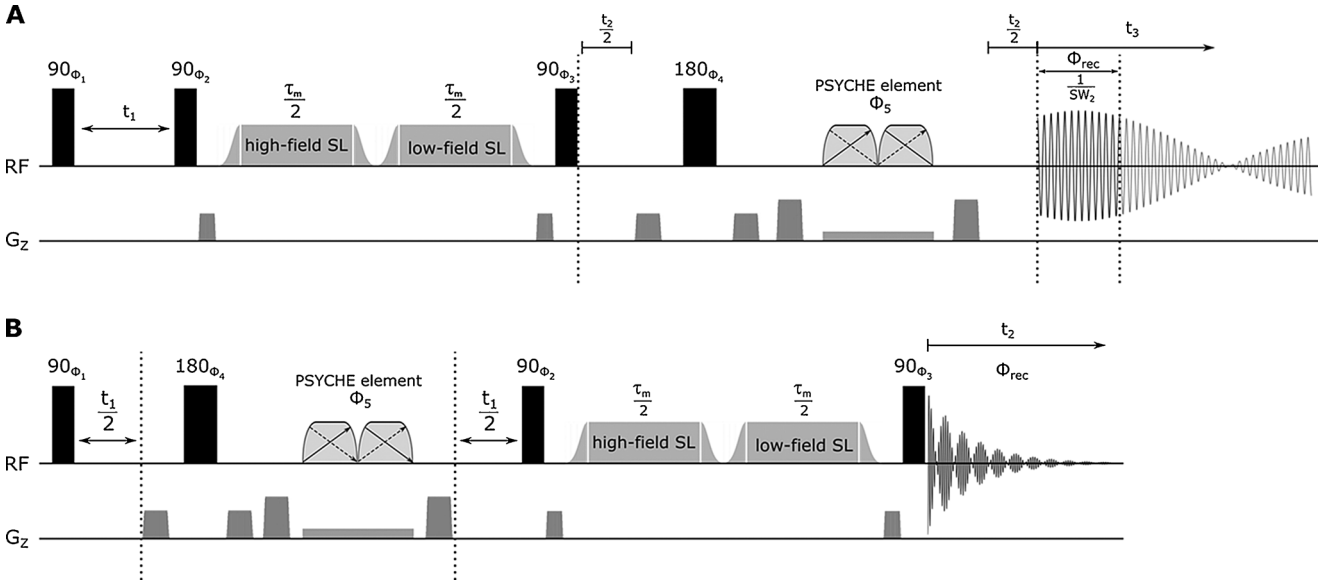

Figure 3. Pulse sequence of PUSH-EASY-ROESY with decoupling in the F_2 (A) and F_1 (B) dimension. Narrow and wide rectangles represent 90° and 180° pulses, respectively. Trapezoids with diagonal arrows correspond to low-power chirp pulses of small flip angle, which sweep frequency in opposite directions simultaneously. Broad rectangles in gray are low- and high-field spinlocks; half-Gaussian shaped pulses were used as adiabatic ramps. For more details see Supporting Information.

approach) to collapse broad multiplets into singlets.[23] We used the PSYCHE[24] experiment (pure shift yielded by chirp excitation) from which we expected the best compromise between decoupling quality and sufficient sensitivity. As homodecoupling simplified NMR signals assignment significantly, the PSYCHE element was implemented into the EASY ROESY pulse sequence. We thus developed two new pure shift EASY ROESY NMR experiments (PUSH-EASY-ROESY, Figure 3), which provide negligible offset dependence combined with an efficient suppression of possible TOCSY transfer artefacts and the improved signal resolution from PSYCHE homodecoupling. In general, the experiment was set up with one dimension decoupled (F_1 or F_2) and then covariance processing[25] (along F_2 or F_1, respectively) was employed to produce a doubly pure shift 2D spectrum. Almost the same results were obtained for the decoupling of either F_1 or F_2, albeit the decoupling in the indirect dimension is less time consuming: the F_1-decoupled PUSH-EASY-ROESY was measured in 26 h whereas the F_2-decoupled experiment took significantly longer. Note that the improved resolution asks for a compromise in sensitivity (typical reduction to 5–20% of the intensity in conventional spectra).

The covariance-processed data provide significantly better resolution (ultra-high-resolved spectra) than Fourier-transform processed spectra (see Supporting Information) and enabled us to detect the intermolecular interaction between the two cyclohexyl moieties of **1** and **2** (Figure 4). For illustration of the intermolecular interactions found we used the computed structure of **1**, which agrees well with RDCs and ROE-based data (one of the four final structures from Figure 1) and added (*R*,*R*)-**2**. The blue arrow in Figure 4 corresponds to the interactions found in PUSH-EASY-ROESY as cross peaks (in the blue frames).

In conclusion, we obtained detailed experimental NMR spectroscopic data that support the results from previously published computational studies. After the conformational analysis of peptide catalyst **1** based on ROE and RDCs, we

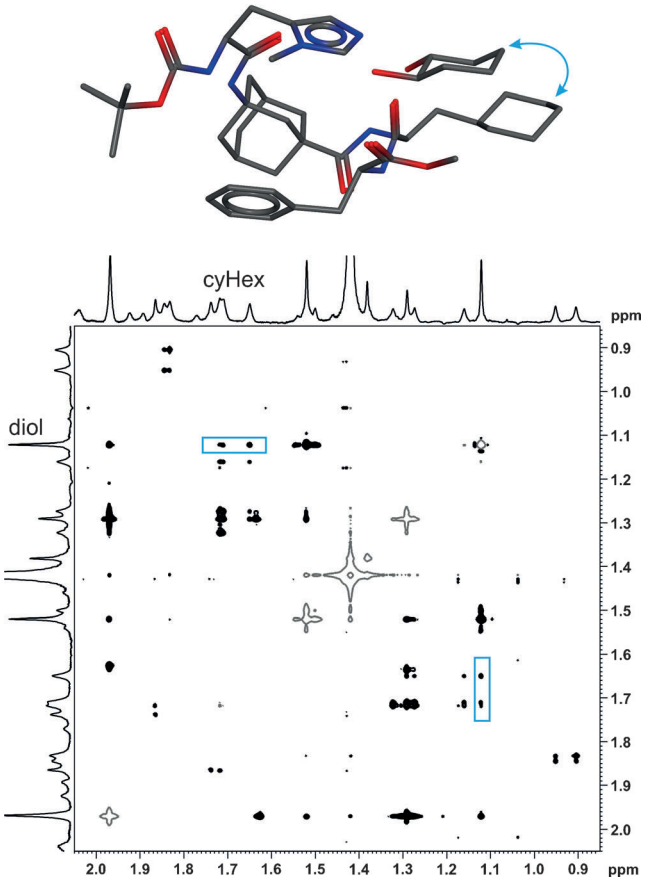

Figure 4. Part of the F_1-PSYCHE-decoupled EASY ROESY spectrum of a mixture of **1** with (*R*,*R*)-**2**. For simplicity, 1D TSE-PSYCHE spectra are shown along both dimensions.

arrived at an ensemble of four pocket-shaped conformations. Probing the interactions between **1** and the two enantiomers of **2** (utilizing T_1 measurements), we showed that catalyst–substrate complex formation occurs; we found a four-times lower T_1 of **2** in a mixture with **1**. These results were supported by DOSY measurements, where we observed that (*R*,*R*)-**2** forms a tighter interaction with **1** than (*S*,*S*)-**2**. From the intramolecular distances extracted from NOE-based data, we assigned significant structural changes in the His part of **1** after the addition of (*R*,*R*)-**2**. Finally, we developed two novel NMR methods, namely EASY ROESY experiments with PSYCHE homodecoupling implemented in the F_1 or F_2 dimension. These techniques enabled the detection of intermolecular dispersion interactions between **2** and the cyclohexyl moiety of **1** despite the overcrowded NMR spectra. This work supports the predicted structural properties, such as dynamic binding-pocket formation of the peptide catalyst **1**, enantiodiscrimination of racemic diol **2**, and crucial intermolecular dispersion interactions. Very interesting chemical shift dependences on concentration were observed, which could open a new field for study of catalyst–substrate complex formation.

Acknowledgements

We thank A.-C. Pöppler for a gift of the thermally cross-linked PS gel and C. E. Müller for performing some of the initial computations. This work was supported by the DFG, Priority Program "Dispersion" (SPP 1807, Schr 597/27-1) and by ERC grant No. 257041 (to C.M.T.).

Keywords: conformational analysis · enantioselective acylations · NMR spectroscopy · pure shift NMR · RDCs

[1] a) C. E. Müller, P. R. Schreiner, *Angew. Chem. Int. Ed.* **2011**, *50*, 6012 – 6042; *Angew. Chem.* **2011**, *123*, 6136 – 6167; b) J. Otera, J. Nishikido, *Esterification: Methods, Reactions, and Applications*, 2nd ed., Wiley, **2010**.
[2] E. Vedejs, M. Jure, *Angew. Chem. Int. Ed.* **2005**, *44*, 3974 – 4001; *Angew. Chem.* **2005**, *117*, 4040 – 4069.
[3] J. B. Jones, *Tetrahedron* **1986**, *42*, 3351 – 3403.
[4] a) S. J. Miller, G. T. Copeland, N. Papaioannou, T. E. Horstmann, E. M. Ruel, *J. Am. Chem. Soc.* **1998**, *120*, 1629 – 1630; b) E. A. C. Davie, S. M. Mennen, Y. J. Xu, S. J. Miller, *Chem. Rev.* **2007**, *107*, 5759 – 5812.
[5] a) S. J. Miller, *Acc. Chem. Res.* **2004**, *37*, 601 – 610; b) H. Wennemers, *Chem. Commun.* **2011**, *47*, 12036 – 12041.
[6] C. E. Müller, L. Wanka, K. Jewell, P. R. Schreiner, *Angew. Chem. Int. Ed.* **2008**, *47*, 6180 – 6183; *Angew. Chem.* **2008**, *120*, 6275 – 6278.
[7] C. E. Müller, D. Zell, R. Hrdina, R. C. Wende, L. Wanka, S. M. Schuler, P. R. Schreiner, *J. Org. Chem.* **2013**, *78*, 8465 – 8484.
[8] C. B. Shinisha, R. B. Sunoj, *Org. Lett.* **2009**, *11*, 3242 – 3245.
[9] Y. Zhao, D. G. Truhlar, *Acc. Chem. Res.* **2008**, *41*, 157 – 167.
[10] D. Neuhaus, M. P. Williamson, *The Nuclear Overhauser Effect in Structural and Conformation Analysis*, second ed., Wiley, Chichester, **2000**.
[11] a) C. M. Thiele, *Eur. J. Org. Chem.* **2008**, 5673 – 5685; b) B. Böttcher, C. M. Thiele, in *Encyclopedia of Magnetic Resonance*, *Vol. 1*, Wiley, Hoboken, **2012**.
[12] K. Stott, J. Stonehouse, J. Keeler, T. L. Hwang, A. J. Shaka, *J. Am. Chem. Soc.* **1995**, *117*, 4199 – 4200.
[13] C. M. Thiele, K. Petzold, J. Schleucher, *Chem. Eur. J.* **2009**, *15*, 585 – 588.
[14] a) H. T. Hu, K. Krishnamurthy, *J. Magn. Reson.* **2006**, *182*, 173 – 177; b) S. Macura, B. T. Farmer, L. R. Brown, *J. Magn. Reson.* **1986**, *70*, 493 – 499.
[15] A. C. Pöppler, H. Keil, D. Stalke, M. John, *Angew. Chem. Int. Ed.* **2012**, *51*, 7843 – 7846; *Angew. Chem.* **2012**, *124*, 7963 – 7967.
[16] A. Enthart, J. C. Freudenberger, J. Furrer, H. Kessler, B. Luy, *J. Magn. Reson.* **2008**, *192*, 314 – 322.
[17] D. Uhrín, G. Batta, V. J. Hruby, P. N. Barlow, K. E. Kövér, *J. Magn. Reson.* **1998**, *130*, 155 – 161.
[18] J. A. Losonczi, M. Andrec, M. W. F. Fischer, J. H. Prestegard, *J. Magn. Reson.* **1999**, *138*, 334 – 342.
[19] a) C. M. Thiele, V. Schmidts, B. Böttcher, I. Louzao, R. Berger, A. Maliniak, B. Stevensson, *Angew. Chem. Int. Ed.* **2009**, *48*, 6708 – 6712; *Angew. Chem.* **2009**, *121*, 6836 – 6840; b) M. Fredersdorf, R. Göstl, A. Kolmer, V. Schmidts, P. Monecke, S. Hecht, C. M. Thiele, *Chem. Eur. J.* **2015**, *21*, 14545 – 14554; c) A. Kolmer, L. J. Edwards, I. Kuprov, C. M. Thiele, *J. Magn. Reson.* **2015**, *261*, 101 – 109.
[20] a) W. L. Jorgensen, J. Tirado-Rives, *J. Am. Chem. Soc.* **1988**, *110*, 1657 – 1666; b) W. L. Jorgensen, D. S. Maxwell, J. Tirado-Rives, *J. Am. Chem. Soc.* **1996**, *118*, 11225 – 11236.
[21] MacroModel, 2012 as contained in Maestro, Version 9.7, SchrödingerLLC, New York, **2014**.
[22] J. P. Wagner, P. R. Schreiner, *Angew. Chem. Int. Ed.* **2015**, *54*, 12274 – 12296; *Angew. Chem.* **2015**, *127*, 12446 – 12471.
[23] K. Zangger, *Prog. Nucl. Magn. Reson. Spectrosc.* **2015**, *86 – 87*, 1 – 20.
[24] M. Foroozandeh, R. W. Adams, N. J. Meharry, D. Jeannerat, M. Nilsson, G. A. Morris, *Angew. Chem. Int. Ed.* **2014**, *53*, 6990 – 6992; *Angew. Chem.* **2014**, *126*, 7110 – 7112.
[25] R. Brüschweiler, F. L. Zhang, *J. Chem. Phys.* **2004**, *120*, 5253 – 5260.

Received: September 1, 2016
Published online: ■■ ■■, ■■■■

Communications

NMR Spectroscopy

E. Procházková, A. Kolmer, J. Ilgen,
M. Schwab, L. Kaltschnee,
M. Fredersdorf, V. Schmidts, R. C. Wende,
P. R. Schreiner,*
C. M. Thiele* ——— ■■■■–■■■■

Uncovering Key Structural Features of an Enantioselective Peptide-Catalyzed Acylation Utilizing Advanced NMR Techniques

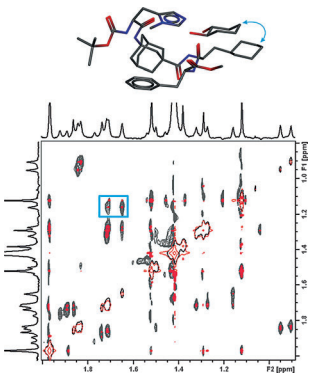

Mission possible: Advanced NMR spectroscopic data support the mechanism proposed for a highly enantioselective acylation reaction. The pocket-like structure of the catalyst is structurally affected upon the addition of the preferentially acetylated diol substrate and key dispersion interactions between catalyst and substrate were uncovered by a newly developed pure shift EASY ROESY experiment.